

Generation of Poincaré beams due to unfolding of fractional optical vortex beams and associated Geometric phase

Satyajit Maji, Aswini K. Pattanayak and Maruthi M. Brundavanam

Department of Physics, Indian Institute of Technology Kharagpur, Kharagpur 721302, West Bengal, India.

Email: satyajitmaji.phy@phy.iitkgp.ac.in

Abstract: Optical vortex beam is generated by the diffraction of a Gaussian beam using computer generated hologram embedded with mixed screw-edge dislocation. Unfolding of the generated fractional vortex beam into eigen-polarization components inside a birefringent crystal results in the conversion of scalar phase singularity to vector polarization singularities in the beam cross-section. The evolution of the singularities of the ellipse field namely C-points (points of undefined major axis) and L-lines (lines of undefined handedness) across the beam quantifies the transformation. The effect of the phase morphology dictated by the fractional order of the dislocation, transverse spatial separation and longitudinal relative phase of the two eigen-beams on determining the complex transverse polarization structure is investigated. The nature of the generated Poincaré beam is also indicated by projecting the states of polarization on to the Poincaré sphere. With increasing order of dislocation from 0.0 to 1.0 in fractional steps and increasing relative phase, the partial Poincaré beam is transformed to a full Poincaré beam. The transformation of the local structure around the C-points is measured through the geometric phase due to the Poincaré sphere contour around the C-points for different dynamic phase difference of the unfolded FOV beams. This study can be useful for different geometric phase based application of optical vortex beams.

Keywords: optical vortex, computer-generated holograms, fractional vortex beam, polarization singularity, geometric phase, vector vortex beam, Pancharatnam-Berry phase, Poincaré beam.

1. Introduction:

A singularity in an optical field being the smallest structure of the field is of utmost important in nanoscale applications e.g. on-chip photonic components or in general light-matter interaction at the nanoscale [1-4]. The singularity in the optical field can be scalar singularity where phase is undefined and intensity is zero or a vector or ellipse field singularity where some parameters quantifying the polarization state is undefined [3, 5]. Studies have been carried out to generate and classify both the scalar and vector singularities to enhance the utility and understanding of these beams [1-21]. Scalar optical vortex (OV) beams with nested phase singularities that carries orbital angular momentum (OAM) have found applications in optical trapping and manipulation of micro-particles [9], robust, high capacity, secure optical communication [10, 11], hybrid entanglement [12] among many others. Their studies have enabled detailed understanding of optical current flow [13] and optical angular momentum [14]. Applications of vector vortex beams with polarization singularities are in engineering point spread function for imaging [15], enhanced sensitivity in polarimetry methods [16] to name a few. Continuing investigation of optical fields embedded with both type of singularities has initiated new fields of study in optical physics like spin-orbit coupling [17], spin and orbital Hall effect [18, 19], chiral light matter interactions [20] to give some examples from a long list.

The strength of the singularity is characterized by some signed numbers like topological charge (TC) for scalar singularities and topological index (TI), Poincaré-Hopf index for ellipse and vector singularities [3]. Scalar OV beams generated from fractional helicoidal phase steps have exclusive topological features which have been theoretically and experimentally investigated [21-23]. The fractional OV (FOV) beams has intricate optical current flow across the beam and both extrinsic and intrinsic OAM [23-25]. The FOV beams have an overall and near-core anisotropic field distribution [26, 27], and a broad OAM spectrum which is useful in high-dimensional entanglement [28], digital spiral imaging [29], novel trapping applications [30]. On the other hand, a spatially inhomogeneously polarized vector vortex beam may contain singularities of ellipse field in a transverse plane, where the major axis and handedness are undefined and are known as C-points and L-lines respectively [3]. On the parameter space of Poincaré sphere the state of polarization (SoP) are projected and spans the surface of the Poincaré sphere. Thus they are called Poincaré beams [31]. The classical non-separable nature [32] and quantum properties of such vector vortex beams [33] are some recent interests.

For a vector optical field, the inhomogeneous polarization distribution can be associated with two phases, one that describes the instantaneous electric field direction with respect to the major axis of the ellipse. And another phase that describes the orientation of the major axis of the ellipse field. The former is the integrable dynamic phase (DP) which is quantized when integrated along a contour and the latter is the non-integrable unbounded geometric phase (GP) [34]. This GP is the Pancharatnam-Berry phase as its origin lies in the manipulation of the SoP of the light. The GP is most important in the context of Poincaré beams and provides a mean of probing the field near the singular points of the ellipse field. Also because of more robustness of GP than DP, it is very useful in the quantum and other applications [35] in science and is the underlying reason for the spin-orbit effects [36] and effects arising from interaction of polarized light with nanostructures [37] and meta-materials [38].

In this study we have exploited the anisotropy of scalar FOV beams to generate and characterize the Poincaré beams. In the current investigation, the scalar FOV beams are first generated using fractional spiral phase encoded mixed screw-edge dislocation (MSED) holograms or fork-cut holograms. The generated scalar FOV beams are passed through a uniaxial birefringent crystal (YVO_4) to convert them to polarization singularities via unfolding due to birefringence [39-42]. The SoP distribution in the transverse plane is obtained from the measurement of spatially resolved Stokes parameters [41]. From the measured Stokes parameters, three scalar Stokes fields are computed and the polarization singularities are described in terms of the singularities of the Stokes fields [40, 41]. The scalar to polarization singularity transformation is demonstrated by the evolution of the C-points and L-lines across the Poincaré beam. The effect of the determining parameters like phase morphology described by the TC [26, 43], beam separation and relative phases of the eigen-beams are exclusively studied and discussed. The GP associated with the spatial polarization around the C-point singularities due to unfolding of different fractional vortex beams are measured. The variation of the GP due to orientation of the optic axis of the crystal is demonstrated by controlled rotation of the birefringent crystal.

Theory:

Fractional OV beams:

An optical vortex beam of integer TC (m) generated by the diffraction of a Gaussian beam from a computer generated Hologram (CGH) with point screw dislocation can be written as [26, 45],

$$u_m(\rho, \phi, z) = \sqrt{\frac{\pi}{2}} e^{im\phi} (-i)^{|m|+1} \exp\left(\frac{ik}{2z} \rho^2\right) \frac{z_R}{z - iz_R} \sqrt{A} \exp(-A) \left[I_{\frac{|m|-1}{2}}(A) - I_{\frac{|m|+1}{2}}(A) \right] \quad (1)$$

where I_ν denotes the modified Bessel function of first kind of order ν , $z_R = \frac{\pi \omega_0^2}{\lambda}$ is the Rayleigh range

$$\text{and } A = \left(\frac{\rho}{z}\right)^2 \frac{k z_R}{4(1 - i \frac{z_R}{z})}.$$

CGHs embedded with fractional spiral phase giving rise to FOV beams in the far-field. The resulting fractional order(α) OV field expressed as a superposition of integer charge vortex fields is given as [21].

$$u_\alpha(\rho, \phi, z) = \frac{\exp[i(z + \pi\alpha)] \sin(\pi\alpha)}{\pi} \sum_{m=-\infty}^{\infty} \frac{u_m(\rho, \phi, z)}{(\alpha - m)} \quad (2)$$

Spatial separation and relative phase due to unfolding inside a birefringent crystal:

In a uniaxial birefringent crystal, the refractive index of the extraordinary component of light, having polarization direction parallel to the optic axis direction, is a function of the angle between the propagation vector of the beam with the optic axis. This phenomenon in addition to the walk-off between the Poynting vector direction and the wave propagation vector direction results in a spatial shift between the extraordinary ray (e-ray) and ordinary ray (o-ray), when the direction of propagation is not parallel or normal to the optic axis direction [40, 46]. This is called unfolding due to birefringence.

The angle made by the ordinary ray (θ_o) and extraordinary ray (θ_e) inside the crystal when the crystal optic axis is normal to the refracting surface of the crystal is given by [46],

$$\tan \theta_o = \frac{\sin \theta}{\sqrt{n_o^2 - \sin^2 \theta}} \quad \text{and} \quad \tan \theta_e = \frac{n_o \sin \theta}{n_e^2 \sqrt{n_e^2 - \sin^2 \theta}}, \quad (3)$$

where the crystal is rotated at an angle θ about the incident beam from the orientation of normal incidence, n_o and n_e are the ordinary and extraordinary refractive indices respectively.

Using this, the spatial separation between the o-ray and e-ray at the crystal output plane can be written as, $\Lambda = t(\tan \theta_o - \tan \theta_e)$, where ' t ' is the thickness of the crystal. Also because of different path taken by the e-ray and o-ray and due to their different refractive indices, there is an optical path length difference between them. The optical path length difference at a normal plane to the propagation direction after the crystal is given as, $\delta l = t(n_o \sec \theta_o - n_e \sec \theta_e) - \Lambda \sin \theta$.

The calculated values of the transverse spatial separation (Λ) and the optical path difference between the e-ray and o-ray of an unfolded OV beam inside a birefringent crystal, for increasing crystal rotation from normal incidence, is shown in Fig. 1 (a) and (b). In (b) a part of the plot (shown in red dashed rectangle) is zoomed in and replotted for visual clarity. Here the n_o and n_e of the YVO₄ crystal is taken which is 15 mm long (i.e. $t = 15\text{mm}$).

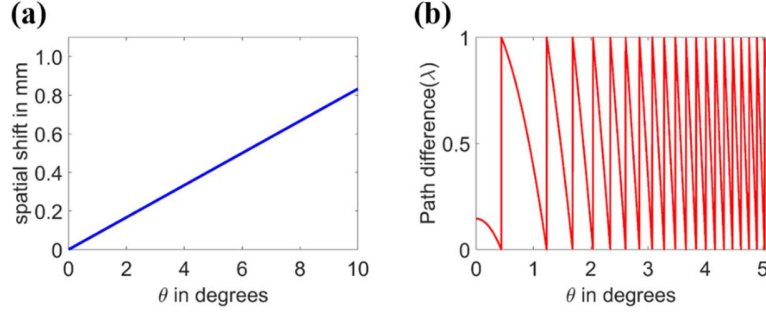


FIG. 1. (a) Transverse spatial shift (Δ) and (b) dynamic phase difference (Δ) between the e-ray and o-ray due to propagation inside a birefringent crystal with optic axis making an angle θ with the propagation direction. Part of the plot in (b) is replotted after zooming in for visual clarity.

Stokes fields due to unfolding of the FOV beams:

The state of polarization at a point across a beam is characterized by four Stokes parameters (s_0, s_1, s_2, s_3), which can be obtained from the six intensity images $I(\beta, \gamma)$ where β and γ are the angle of the quarter-wave-plate and polarizer respectively. From the normalized Stokes parameters (S_0, S_1, S_2, S_3), three complex scalar stokes field (S_{12}, S_{23}, S_{31}) can be constructed by $S_{mn} = S_m + iS_n$. The orientation field i.e. orientation of the major axis (ψ) of the polarization ellipse is obtained from argument of the S_{12} and the relative phase (δ) between the eigen-beams is obtained from argument of the S_{23} as follows [40].

$$\begin{aligned}\psi &= \frac{1}{2} [\tan^{-1}(\frac{S_2}{S_1})] \\ \varphi &= \frac{1}{2} \tan^{-1} \left(\frac{(S_1^2 + S_2^2)^{1/2}}{S_3} \right) \\ \chi &= \frac{\pi}{4} - \varphi \\ \delta &= \frac{1}{2} [\tan^{-1}(\frac{S_3}{S_2})]\end{aligned}\tag{4}$$

The angular parameter (ψ, φ) spans the parameter space of Poincaré sphere (PS) which has radius $S_0 = 1$ and S_1, S_2, S_3 as three axes. $S_3 = \pm 1$ represent the poles and S_1S_2 plane is the equatorial plane. The parameter χ express the ellipticity of the ellipse. C-point singularity is denoted by $\chi = \pm \pi/4$ i.e. $2\varphi = (0, \pi)$ where ψ is undefined and projects to the pole of PS. The L-line is expressed by $S_3 = 0$ and given by $2\varphi = \pi/2$. The upper hemisphere represents left handed ellipses and the lower hemisphere represents right handed ellipses separated by the handedness singularity L-line along the equator. The polarization ellipse and the corresponding SoP parameters on the PS is shown in Figs. 2. (a) and (b), respectively.

Geometric phase associated with transverse polarization structure:

The SoP along any closed path on the real space on the inhomogeneously polarized Poincaré beams also traces a closed loop on the spherical surface of the PS. When the circular path is taken around the C-point singularities in the real space, the PS contour always encloses the S_3 axis. The half of the oriented area (solid angle) enclosed by the PS contour gives the value of the associated GP [34]. For a vectorial electric field distribution represented by $\mathbf{E}(\mathbf{r}) = E(\mathbf{r}) \mathbf{e}(\mathbf{r})$, the geometric phase is given by,

$$\Omega_G = \text{Im} \oint [\mathbf{e}^* \cdot (\nabla) \mathbf{e}] \cdot d\mathbf{r} = \oint (1 \mp \cos(2\varphi)) d\psi \quad (5)$$

Where $\mathbf{e}(\mathbf{r})$ is the unit vector representing the polarization state at point ‘r’ on the orthogonal plane about the beam propagation. The ‘-ve’ sign is for the PS contour around the north pole (in this case around the star C-point) and ‘+ve’ sign is for the PS contour around the south pole (here it is around lemon C-point). The expression of Ω_G in terms the SoP parameters is employed to calculate the area on the PS surface within the PS contour. The process is indicated in Fig. 2(c) and explained as following.

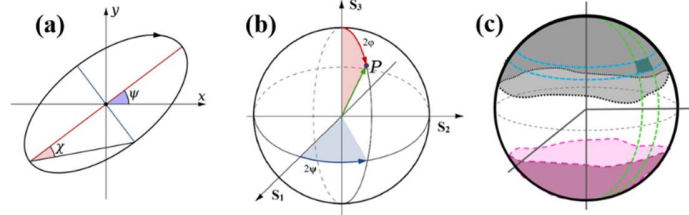


FIG. 2. (a) Polarization ellipse and (b) Poincaré sphere on which the SoP is represented by the point P with parameters that correspond to its semi-polar and semi-azimuthal angles on the sphere. (c) The symbolic representation of the trace of the SoP along a circle around star and lemon C-points (shown in black and magenta dotted line respectively) on the Poincaré sphere and to calculate the oriented surface area (gray and magenta) enclosed by the projected contours.

From the SoP parameter ψ and φ calculated along the circular path around the C-point, the angular coordinate of the points on PS contour is known. As the north hemisphere of the PS represents left-handed polarization and the south hemisphere represents right-handed polarization, the area enclosed by the PS contours is given by the area within the north pole and the contour traced by black dotted line and the area within south pole and the contour traced by magenta dashed lines. In calculating the GP enclosed by the PS contours, the geometric angular coordinates (2φ , 2ψ) of the data points on PS is employed in numerically integrating or summing the infinitesimal spherical surface elements within the contours following Eq. (5).

2. Experimental details:

The experimental setup used to generate Poincare beams is shown in Fig. 3. The diffracted beam from the fractional order CGH displayed on the spatial light modulator (SLM) results in the envisaged scalar FOV beam in the first diffraction order [26]. The generated scalar FOV beam is collimated and polarization is made diagonal. Then the beam is made to pass through a c-cut uniaxial birefringent Yttrium vanadate (YVO_4) crystal placed on a micro-radian precision rotational stage. The dimension of the crystal is 15 mm(length) X 10 mm(width) X 10 mm(height). The optic axis of the crystal lies in the horizontal y-z plane but is rotated about x axis and making an angle θ with z axis. The FOV beam is unfolded upon entering the crystal surface and are spatially separated at the output plane in two orthogonally polarized eigen-beams. The spatial separation of the beam can be controlled by the angle (θ) of optic axis with z axis. Though any change of this angle will also introduce a relative longitudinal optical path difference between the two orthogonal polarized beams. This relative dynamic phase difference is found and demonstrated to be most dominant factor among all the factors controlling the nature of the generated Poincaré beams.

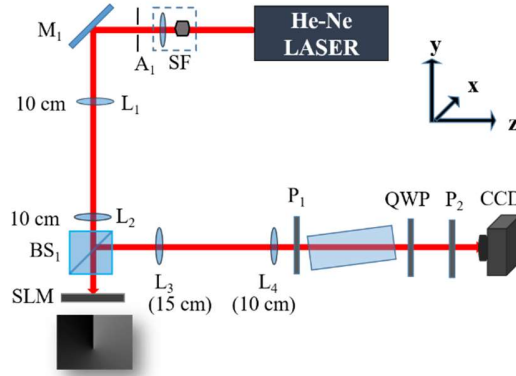


FIG. 3. Generation of spatially inhomogeneous polarized (Poincaré) beam via unfolding of a fractional OV beam in a birefringent (YVO₄) crystal. SF: spatial filter, SLM: spatial light modulator, QWP: quarter-wave-plate, P: polariser.

To measure and vary the longitudinal relative phase (Δ) between the two eigen beams, first the orientations of the crystal giving rise to effective zero (modulo π) phase difference are found by rotating the crystal within a crossed. At these orientations of the crystal, the output intensity profiles show a dark line at the centre of the beam where the phase difference between the eigen-beams is zero modulo π . Assuming the phase difference to be approximately linear with θ for very small change between two consecutive effective zero phase difference configurations, any arbitrary relative phase difference (Δ) between the eigen-beams can be employed within the experimental accuracy. The beam size is measured using 2D Gaussian fitting and the beam separation is calculated using both centre of the fitted Gaussian and centre of intensity calculation at the CCD plane.

The output state of polarization (SoP) at a particular orientation of the crystal is measured by spatially resolved Stokes polarimetry using a QWP and polarizer combination. The spatial variation of SoP is measured with varying beam separation (Δ) and dynamic relative phase (Δ) for different fractional order (α) of the OV beams. The measured relative phase (δ) between the eigen-polarizations will be different from the given longitudinal relative phase (Δ) for any beam that does not have a planar wavefront (for $\alpha \neq 0.0$).

3. Results:

The unfolding of the FOV beam inside an anisotropic medium in to two orthogonal polarized components, results in the output SoP as shown in Fig. 4. In the SoP distributions, red and green ellipses imply right and left handed polarization states respectively and the blue line represents the L-line. The orientation fields (ψ) with polarization streamlines and corresponding spatial distribution of relative phase (δ) derived from the constructed Stokes field using Eq. (4) are also shown.

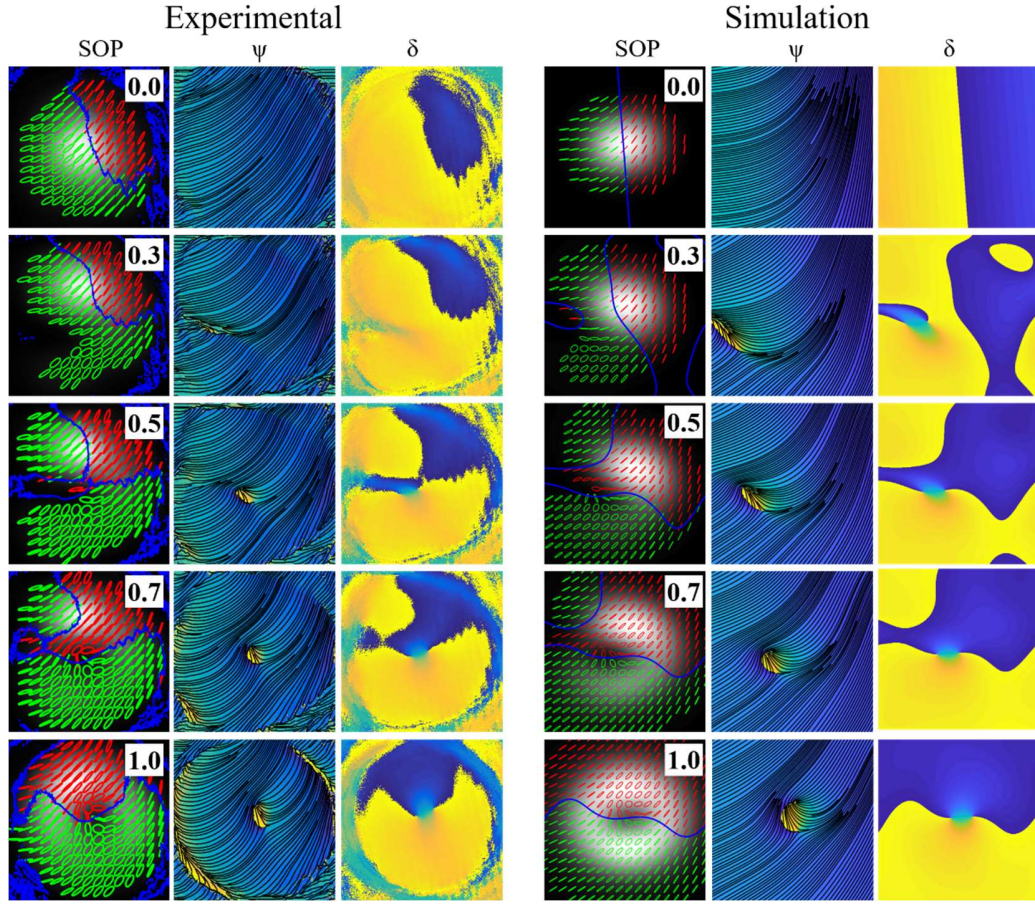


FIG. 4. Unfolding of FOV: Experimental and simulation plots for some values of α between 0.0 and 1.0. SoP across the beam where red and green ellipse represents right and left handedness and the blue line is L-line. Orientation of the ellipse major axis (ψ) with the singularities representing C-points and polarization streamlines describing index of the C-point. Transverse distribution of relative phase (δ) between the two eigen components are shown in the last columns.

The C-points and L-lines are also obtained from the measured Stokes parameters. The points of intersection of the zero contours of S_1 , S_2 as obtained from the singularities of the orientation field $\psi = \text{Arg}(S_{12})$ gives the C-points. The L-lines are drawn as zero contours of S_3 . The singularities of the orientation field clearly show the C-points. The nature of the C-point singularity (lemon or star) is revealed by the polarization streamlines. Three streamlines merging at the C-point implies a star singularity and a single streamline ending at the C-point implies a lemon singularity.

The SoP distribution at the output plane is also simulated by superposing two orthogonal polarized FOV beams using the calculated and measured beam separation and dynamic relative phase from experiments and using Eq. (1) and Eq. (2). It is observed that the number and type of C-point singularities depends on the topological charge of the beam, the spatial separation of the eigen-polarized beams at the output plane and also on the longitudinal relative phase difference between the beams. In the presented results in Fig. 4, the beam separation (Δ) is $0.4w$ (where w is the Gaussian beam radius) and the longitudinal relative phase is zero. The measured value δ matches with the given dynamic phase difference Δ for the Gaussian beam with planar wavefront. The experimental results are well supported by simulation.

Fig. 5 shows the variation of the three angular parameters characterizing the SoP along a circle centred on the C-points with the azimuthal angle of the local coordinate frame where the origin is placed on the C-point. The variation of the parameter ψ when going counter-clockwise along a circle centred on a C-points, dictates the sign of the C-point index. The sign of the C-point index is positive for increasing ψ representing lemon and negative for decreasing ψ representing star. This experimentally measured and calculated values of the SoP parameters are also used later to plot the contours on the PS and calculating the oriented area enclosed by the PS contour.

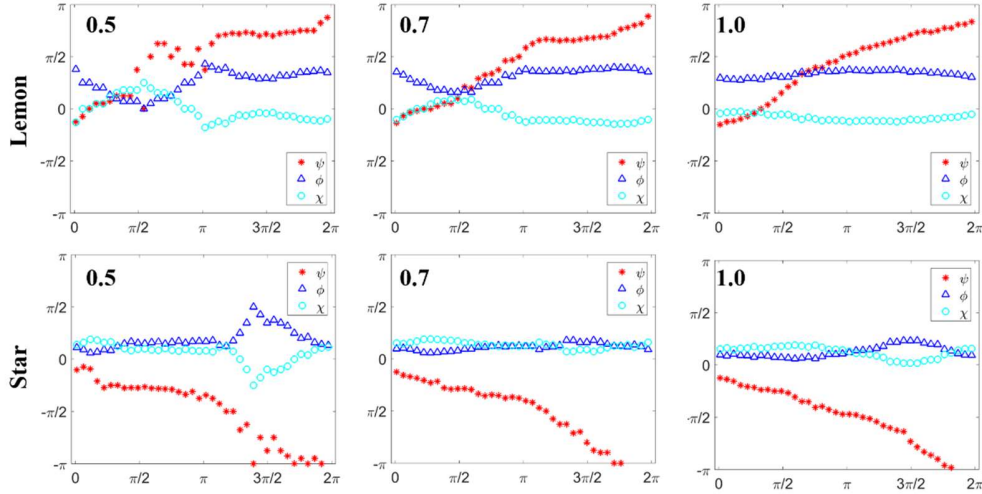


FIG. 5. Variation of the SoP parameters (ψ , χ , ϕ) along the circle around the two C-points for the Poincaré beams generated by unfolding of FOV beams with $\alpha = 0.5, 0.7$ and 1.0

It is observed that, for any $\alpha \geq 0.5$ when the dynamic relative phase due to longitudinal path difference is zero (modulo π) between the two eigen polarized beams, the number of C-points within the beam cross-section is always two: one right-handed lemon and another left handed star C-point singularities. Thus the total index which is the sum of the product of the sign of the C-point index ('+' for lemon and '-' for star) and sign of the handedness index ('+' for right-handed and '-' for left-handed) [39], matches with the total topological charge of the scalar vortex as both equals positive two. The C-points enters within the beam cross-section through the opening of L-line formed near the lower intensity regions corresponding to the edge dislocation of the hologram at $\alpha = 0.5$. With increasing α in fractional steps, the C-points move towards the beam centre and reaches the centre at $\alpha = 1.0$.

When the relative phase difference (Δ) between the eigen beams are changed by a very small rotation of the crystal, the SoP across the beam are observed to pass through a rapid cycle of change. In the following Fig. 6, the effect of beam separation (Λ) and relative phase (Δ) on the SoP is shown in (a) and (b) respectively for FOV of $\alpha = 0.5$. In (a) for demonstrating the effect of change in Λ , Δ is fixed at $2\pi/3$ and in (b) for showing the effect of Δ , Λ is fixed at $0.4w$. It is clearly observed that the nature of the Poincaré beam greatly depends on the value of Δ .

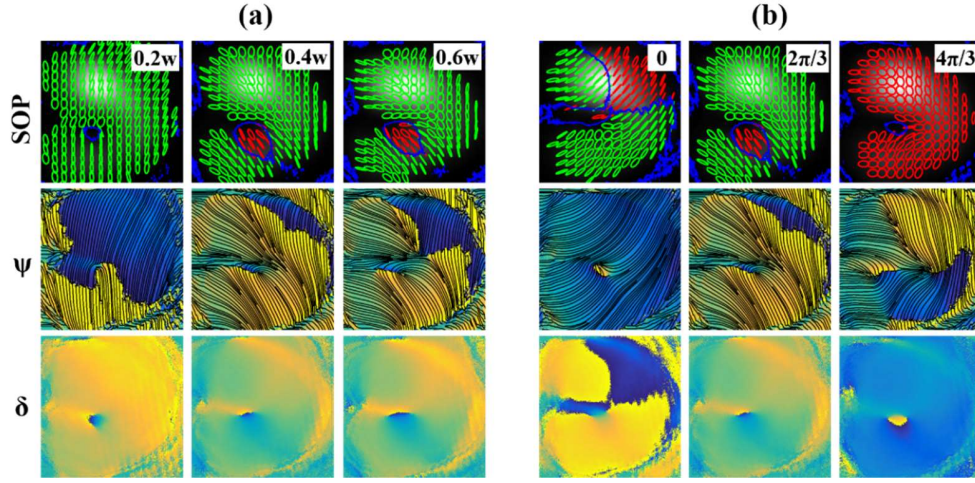


FIG. 6. (a) Effect of beam separation (Δ) for a fixed relative phase ($\Delta=2\pi/3$) and (b) effect of relative phase (Δ) for a fixed beam separation ($\Delta=0.4w$) on the SoP distribution of generated Poincaré beams via unfolding of an OV beam ($\alpha=0.5$).

Below $\alpha = 0.5$, there are no C-points across the beam cross-section. So if all the SoP across the beam is projected on the PS, it will not be sufficient to span the whole surface of the PS. In this cases, the generated Poincaré beam is a partial Poincaré beam. For $0.5 \geq \alpha \leq 1.0$, at $\Delta=0$, there are two C-points that are separated by a L-line. Though the SoP across the beam now span the poles of the PS, the open L-line indicates that it is still insufficient to cover the whole surface of the PS. With increasing relative phase (Δ) at a fixed beam separation, the L-line turns into a closed loop enclosing one C-point after some critical value of Δ . When the L-line encloses one C-point forming a closed loop within the beam cross-section, then the SoP across the beam span the full PS and the beam now becomes a full Poincaré beam. So with varying α and Δ , it is possible to transform a partial Poincaré beam in to a full Poincaré beam.

It is also observed that a new pair of C-points: one star and one lemon, of the same handedness may arise in the beam cross section after some critical beam separation. The new pair of C-points both being of same handedness does not contribute to the total index as they have opposite sign of the C-point index. And the L-line encloses one out of two (or four) C-points: either one right-handed lemon or a left-handed star. The following table (Table 1) summarizes the number and index of the C-points observed.

Table 1: Number and index of C-points for some relative phase and beam separation of the eigen beams (magenta circle: Lemon; Black star: Star; d: degenerate state for distribution of C-points)

Δ/w \ δ	0	$\pi/2$	$2\pi/3$	$3\pi/2$	$4\pi/3$
0.2	● ★	d	● ★	d	● ★
0.4	● ★	d	● ★	d	● ★ ○ ★
0.6	● ★	d	● ★ ○ ★	d	● ★ ○ ★

The L-line is an open line intersecting the beam in half when the relative phase is around 0 or π and move very rapidly across the beam. This correspond to the degenerate case for the L-line singularity as a relative phase of 0 or π between two orthogonal linear polarization components gives a linear polarization. For any other relative phase, the L-line very rapidly takes a closed loop form and encloses a C-point

singularity near the beam centre as explained earlier. When the phase difference approaches near $\pi/2$ or $3\pi/2$, the SoP across most of the beam cross-section is close to circular polarization and the beam is found to be embedded with three C-points. In this cases, the new C-points move very rapidly across the beam with slight change of Δ . This is denoted by a ‘degenerate’ {d} condition as a relative phase of $\pi/2$ between two orthogonal polarization gives circular polarization state in table 1.

To study the nature of the Poincaré beam, the SoP around the C-points are projected on the PS. As already mentioned, on the PS, the poles are C-points and the equator spans the L-line and separates the right-handed and left-handed SoPs. So, SoP along any circle around one of C-points traces a circle around one of the pole. The position, orientation and tilt of the contour on the PS, about the equator is a qualitative measure of the local structure of the C-point singularity as it describes the variation of the SoP around the C-point [34, 47]. This are shown in Figs. 7 and 8 for varying α , Λ and Δ and explained below.

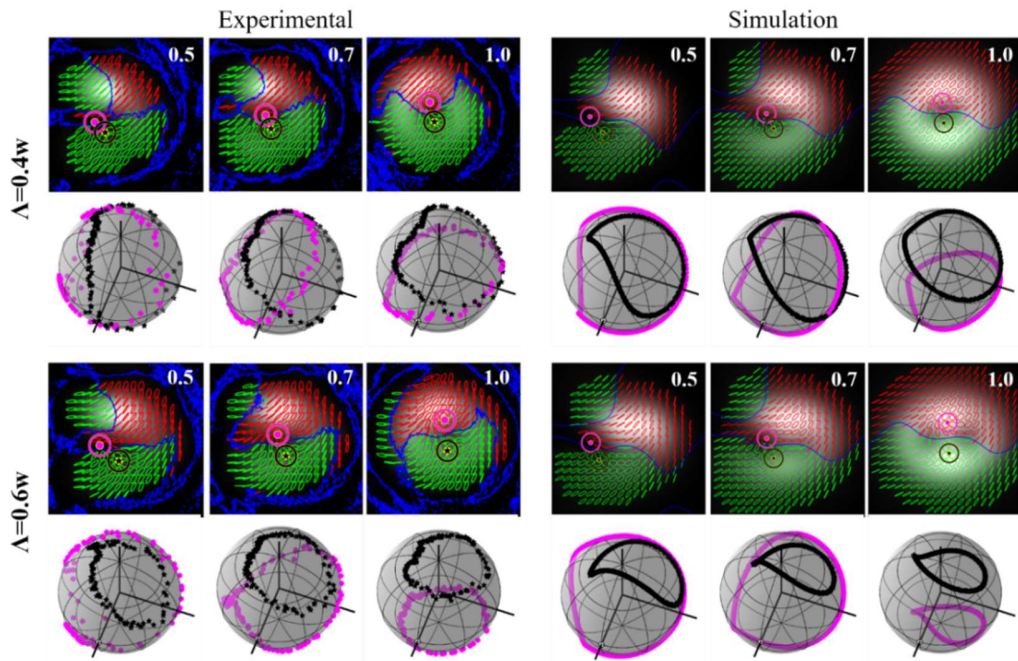


FIG. 7. Projection of SoP along a circle around the C-points on the Poincaré sphere for beam separation: $\Lambda=0.4w$ and $0.6w$ (w is the Gaussian beam radius) for $\alpha= (0.5, 0.7$ and $1.0)$; $\Delta=0$.

In Fig. 7, the effect of varying the beam separation (Λ) for a particular relative phase ($\Delta=0$) is shown. The lemon and star are shown with a magenta circle and black star whereas the circle along which the SoP parameters are calculated are shown in magenta and black line. The projection of SoP around the lemon and star on the PS is shown in magenta circles and black stars respectively. With increasing separation, the inhomogeneity of the SoP around the C-points decreases and the circle on the PS transits towards a geodesic of the sphere. In Fig. 8 the effect of varying relative phase (Δ) for a particular the beam separation ($\Lambda = 0.4w$) is shown.

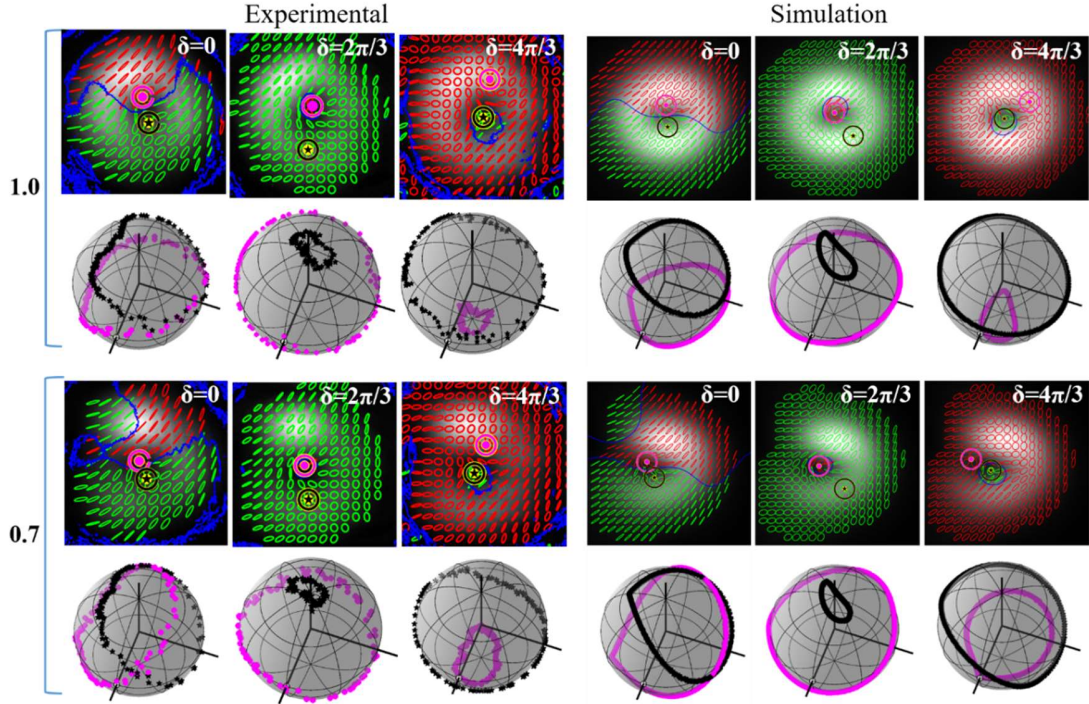


FIG. 8: Projection of SoP along a circle around the C-points on the Poincaré sphere for varying relative phases: $\Delta=0, 2\pi/3$ and $4\pi/3$; For $\alpha= 0.7, 1.0$; $\Lambda=0.4w$ (w is the Gaussian beam radius).

The enclosed spherical surface area by the Poincaré sphere (PS) contour is a measure of the GP associated with the C-point singularity [34]. The variation of the GP due to the PS contour calculated using Eq. (5) for different fractional values of α is shown with varying relative phases in Fig. 9 (a). Though the actual amount of GP is dependent on the radius of the circular path chosen around the C-points but the qualitative nature of the variation with α is same.

In Fig. 9(a), magenta circle represents GP for lemon C-points whereas black star represents GP for star C-points. The plot of GP with α for different value of Δ reveals that variation is maximum for $\Delta = 0$ and least for $\Delta = 2\pi/3$ where GP is almost independent of α .

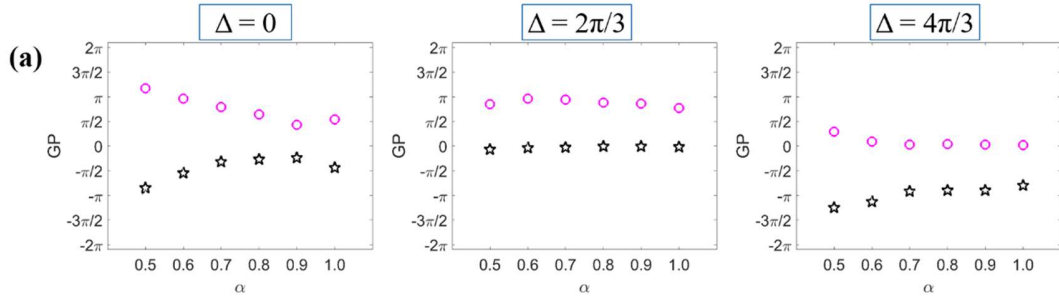


FIG. 9. (a) Variation of the geometric phase enclosed by the PS contour with varying α for $\Delta = 0, 2\pi/3$ and $4\pi/3$ at $\Lambda=0.4w$.

5. Conclusion:

In summary, scalar fractional optical vortex beams are generated using computer generated holograms embedded with fractional helicoidal phase step. By unfolding the generated diagonally polarized FOV beams inside a uniaxial birefringent crystal, Poincaré beams are generated at the output of the crystal due to the spatial walk-off of the eigen-polarizations. The output transverse polarization distribution implies the scalar phase singularities of the input beam are transformed to polarization singularities. The complex phase structure of the FOV beams, the transverse beam separation of the eigen-polarizations and their longitudinal relative phases, all of this are a major factor in determining the complex polarization structure of the generated Poincaré beams. The fractional order of the of the CGH determines the phase structure and local anisotropy of the vortices which themselves can be mapped to a morphology sphere in analogy to the Poincaré sphere [43]. The beam separation and the relative phase of the two eigen-polarizations determines the number and index of C-points within the beam cross-section and the area of the unfolding region of the unfolded vortex beams. This study can be useful in engineering the point spread functions for imaging and in metrology. The classical ‘entanglement’ or non-separability of the polarization and spatial mode degrees of freedom in Poincaré beams is a promising feature to be useful in classical realization of some algorithm exploiting the entanglement feature of quantum systems. This study may help in realizing the controlled degree of classical entanglement which requires further investigation of these beams.

Acknowledgments:

This research work is supported by Department of Science and Technology (DST), India with grant number (INSPIRE Faculty Award/2013/PH-62) and Indian Institute of Technology Kharagpur (IITKGP), India with grant number (IIT/SRIC/PHY/VBC/2014-15/43).

ORCID iDs

Satyajit Maji: <https://orcid.org/0000-0002-9432-7615>

Maruthi M Brundavanam: <https://orcid.org/0000-0003-0442-3599>

References:

- [1] J. F. Nye and M. V. Berry, Dislocations in wave trains, *Proc. R. Soc. A* **336**, 165 (1974).
- [2] M. Buresi, R. J. P. Engelen, A. Opheji, D. van Oosten, D. Mori, T. Baba, and L. Kuipers, Observation of polarization singularities at the nanoscale, *Phys. Rev. Lett.* **102**, 033902 (2009).
- [3] M. R. Dennis, K. O’Holleran, and M. J. Padgett, Chapter 5, Singular Optics: Optical vortices and polarization singularities. *Progress in Optics*, **53**, 293 (2009).
- [4] L. T. Vuong, A. J. L. Adam, J. M. Brok, P. C. M. Planken, and H. P. Urbach, Electromagnetic Spin-Orbit interactions via scattering of subwavelength apertures, *Phys. Rev. Lett.* **104**, 083903 (2010).
- [5] S. K. Pal, Ruchi, and P. Senthilkumaran, C-point and V-point singularity lattice formation and index sign conversion methods, *Opt. Commun.* **393**, 156 (2017).
- [6] R. P. Singh and S. R. Chowdhury, Trajectory of an optical vortex: canonical vs. non-canonical, *Opt. Commun.* **215**, 231 (2003).
- [7] I. Freund and V. Freilikher, Parametrization of anisotropic vortices, *J. Opt. Soc. Am. A* **14**, 1902 (1997).
- [8] M. R. Dennis, Polarization singularity anisotropy: determining monstardom, *Opt. Lett.* **33**, 2572 (2008).
- [9] K. T. Gahagan and G. A. Swartzlander Jr., Optical vortex trapping of particles, *Opt. Lett.* **21**, 827 (1996).
- [10] A. E. Willner et al, Optical communications using orbital angular momentum beams, *Adv. Opt. Photonics* **7**, 66 (2015).
- [11] S. Mi, T. Wang, G. Jin, C. Wang, High capacity quantum secure direct communication with orbital angular momentum of photons, *IEEE J. Phot.* **7**, 7600108 (2015).

- [12] J. T. Barreiro, N. K. Langford, N. A. Peters, and P.G. Kwiat, Generation of hyper-entangled photon pairs, *Phys. Rev. Lett.* **95**, 260501 (2005).
- [13] M. V. Berry, Optical currents, *J. Opt. A: Pure Appl. Opt.* **11**, 094001 1-12 (2009).
- [14] A. M. Yao and M. J. Padgett, Orbital angular momentum: origins, behaviour and applications, *Advances in Optics and Photonics* **3**, 161-204 (2011).
- [15] R. Dorn, S. Quabis, and G. Leuchs, Sharper focus for a radially polarized light beam, *Phys. Rev. Lett.* **91**, 233901 (2003).
- [16] F. Toppel et. Al, Classical entanglement in polarization metrology, *New J. Phys* **16**, 073019 (2014).
- [17] L. Marucci, C. Manzo, and D. Paparo, Optical spin to orbital angular momentum conversion in inhomogeneous anisotropic media, *Phys. Rev. Lett.* **96**, 163905 (2006).
- [18] M. Onoda, S. Murakami, and N. Nagaosa, Hall effect of light, *Phys. Rev. Lett.* **93**, 083901 (2004).
- [19] O. Hosten and P. Kwiat, Observation of the spin Hall effect of light via weak measurements, *Science* **319**, 787 (2008).
- [20] R. P. Cameron, J. B. Götte, S. M. Barnett, and A. M. Yao, Chirality and the angular momentum of light, *Phil. Trans. R. Soc. A* **375**, 20150433 (2016).
- [21] M. V. Berry, Optical vortices evolving from helicoidal integer and fractional phase steps, *J. Opt. A: Pure Appl. Opt.* **6**, 259 (2004).
- [22] J. Leach, E. Yao, and M. J. Padgett, Observation of the vortex structure of a non-integer vortex beam, *New J. Phys.* **6**, 71 (2004).
- [23] S. Maji and M. M. Brundavanam, Topological transformation of fractional optical vortex beams using computer generated holograms, *J. Opt.* **20**, 045607 (2018).
- [24] S. N. Alperin and M. E. Siemens, Angular momentum of topologically structured darkness, *Phys. Rev. Lett* **119**, 203902 (2017).
- [25] A. T. O’Neil, I. MacVicar, L. Allen, and M. J. Padgett, Intrinsic and Extrinsic Nature of the Orbital Angular Momentum of a Light Beam, *Phys. Rev. Lett.* **88**, 053601 (2002).
- [26] S. Maji and M. M. Brundavanam, Controlled non-canonical vortices from higher order fractional screw dislocation, *Opt. Lett.* **42**, 2322 (2017).
- [27] S. Maji, A. Mandal, and M. M. Brundavanam, Gouy phase-assisted topological transformation of vortex beams from fractional fork holograms, *Opt. Lett.* **44**, 2286 (2019).
- [28] S. S. R. Oemrawsingh, X. Ma, D. Voigt, A. Aiello, E. R. Eliel, G. W’t Hooft and J. P. Woerdman, Experimental demonstration of fractional orbital angular momentum entanglement of two photons, *Phys. Rev. Lett.* **95**, 240501 (2005).
- [29] L. Chen, J. Lei, and J. Romero, Quantum digital spiral imaging, *Light: Science & Applications* **3**, 153 (2014).
- [30] S. H. Tao, X-C Yuan, J. Lin, X. Peng, and H. B. Niu, Fractional optical vortex beam induced rotation of particles, *Opt. Express* **13**, 7726-7731 (2005).
- [31] A. M. Beckley, T.G. Brown, and M. A. Alonso, Full Poincaré beams, *Opt. Express* **18**, 10777 (2010).
- [32] R. J. C. Spreeuw, A classical analogy of entanglement, *Found. Phys.* **28**, 3 361 (1998).
- [33] R. Fickler, R. Lapkiewicz, S. Ramelow, and A. Zeilinger, Quantum entanglement of complex photon polarization patterns in vector beams, *Phys. Rev. A* **89**, 060301 (2014).
- [34] K. Y. Bliokh, M. A. Alonso, and M. R. Dennis, Geometric Phases in 2D and 3D polarized fields: geometrical, dynamical and topological aspects, *arxiv* 1903.01304 (2019).
- [35] A. Bohm, A. Mostafazadeh, H. Koizumi, Q. Niu, and J. Zwanziger, The geometric phase in quantum systems: Foundations, Mathematical concepts, and applications in molecular and condensed matter physics, Springer (2003).
- [36] S-L Zhu and P. Zanardi, Geometric quantum gates that are robust against stochastic control errors, *Phys. Rev. A* **72**, 020301(R) (2005).
- [37] K. Y. Bliokh, F. J. Rodríguez-Fortuño, F. Nori, and A. V. Zayats, Spin-orbit interactions of light, *Nature Photon.* **9**, 796 (2015).
- [38] A. E. Minovich and A. V. Zayats, Geometric-phase metasurfaces based on anisotropic reflection: generalized design rules, *ACS Photonics* **5**, 1755-1761 (2018).
- [39] K. Y. Bliokh, Y. Gorodetski, V. Kleiner, and E. Hasman, Coriolis effect in optics: unified geometric phase and Spin-Hall effect, *Phys. Rev. Lett.* **101**, 030404 (2008).
- [40] F. Flossman, U. T. Schwarz, M. Maier, and M. R. Dennis, Singularities from unfolding an optical vortex through a birefringent crystal, *Phys. Rev. Lett.* **95**, 253901 (2005).
- [41] M. M. Brundavanam, Y. Miyamoto, R. K. Singh, D. N. Naik, M. Takeda, and K. Nakagawa, Interferometer setup for the observation of polarization structure near the unfolding of an optical vortex beam in a birefringent crystal, *Opt. Express* **20**, 13573 (2012).

- [41] F. Flossman, U. T. Schwarz, M. Maier, and M. R. Dennis, Stokes parameters in the unfolding of an optical vortex through a birefringent crystal, *Opt. Express* **14**, 11402 (2006).
- [42] A. K. Pattanayak, S. Maji, and M. M. Brundavanam, Polarization singularities due to unfolding of fractional vortex beams in a birefringent crystal, JTU3A.91, *OSA technical digest, Frontiers in Optics 2017*, Washington DC, USA.
- [43] S. Maji and M. M. Brundavanam, Evolution of an optical vortex on the morphology sphere by control of fractional charge of the dislocation, JTU3A.82, *OSA technical digest, Frontiers in Optics 2017*, Washington DC, USA.
- [44] N. W. M. Ritchie, J. G. Story, and R. G. Hulet, Realization of measurement of a “weak value”, *Phys. Rev. Lett.* **66**, 1107 (1991).
- [45] A. Y. Bekshaev and A. I. Karamoch, Spatial Characteristics of vortex light beams produced by diffraction gratings with embedded phase singularity, *Opt. Commun.* **281**, 1366 (2008).
- [46] M. Avedaño-Alejo, Analysis of the refraction of the extraordinary ray in a plane-parallel uniaxial plate with an arbitrary orientation of the optic axis, *Opt. Express* **13**, 2549 (2005).